MOLECULAR IMAGING AND BIOLOGY

Mol Imaging Biol (2016) 18:18–23
DOI: 10.1007/s11307-015-0862-4

Published Online: 14 May 2015

BRIEF ARTICLE

Preclinical Evaluation of 4-[^{18}F]Fluoroglutamine PET to Assess ASCT2 Expression in Lung Cancer

Mohamed Hassanein,[1,2] Matthew R. Hight,[3,4] Jason R. Buck,[3,4] Mohammed N. Tantawy,[3,4] Michael L. Nickels,[3,4] Megan D. Hoeksema,[1] Bradford K. Harris,[1] Kelli Boyd,[5] Pierre P. Massion,[1,2,6] H. Charles Manning[3,4,6,7]

[1]*Division of Allergy, Pulmonary and Critical Care Medicine, Vanderbilt University School of Medicine, Nashville, TN, 37232, USA*
[2]*Thoracic Program, Vanderbilt-Ingram Cancer Center, Vanderbilt University Medical Center, Nashville, TN, 37232, USA*
[3]*Vanderbilt University Institute of Imaging Science (VUIIS), Vanderbilt University Medical Center, Nashville, TN, 37232, USA*
[4]*Department of Radiology and Radiological Sciences, Vanderbilt University Medical Center, Nashville, TN, 37232, USA*
[5]*Department of Pathology, Microbiology and Immunology, Vanderbilt University Medical Center, Nashville, TN, 37232, USA*
[6]*Vanderbilt-Ingram Cancer Center, Vanderbilt University Medical Center, Nashville, TN, 37232, USA*
[7]*Program in Chemical and Physical Biology, Vanderbilt University Medical Center, Nashville, TN, 37232, USA*

Abstract

Purpose: Alanine-serine-cysteine transporter 2 (ASCT2) expression has been demonstrated as a promising lung cancer biomarker. (2*S*,4*R*)-4-[^{18}F]Fluoroglutamine (4-[^{18}F]fluoro-Gln) positron emission tomography (PET) was evaluated in preclinical models of non-small cell lung cancer as a quantitative, non-invasive measure of ASCT2 expression.

Procedures: In vivo microPET studies of 4-[^{18}F]fluoro-Gln uptake were undertaken in human cell line xenograft tumor-bearing mice of varying ASCT2 levels, followed by a genetically engineered mouse model of epidermal growth factor receptor (EGFR)-mutant lung cancer. The relationship between a tracer accumulation and ASCT2 levels in tumors was evaluated by IHC and immunoblotting.

Result: 4-[^{18}F]Fluoro-Gln uptake, but not 2-deoxy-2-[^{18}F]fluoro-D-glucose, correlated with relative ASCT2 levels in xenograft tumors. In genetically engineered mice, 4-[^{18}F]fluoro-Gln accumulation was significantly elevated in lung tumors, relative to normal lung and cardiac tissues.

Conclusions: 4-[^{18}F]Fluoro-Gln PET appears to provide a non-invasive measure of ASCT2 expression. Given the potential of ASCT2 as a lung cancer biomarker, this and other tracers reflecting ASCT2 levels could emerge as precision imaging diagnostics in this setting.

Key words: Glutamine, PET, SLC1A5, ASCT2, Transporter, NSCLC, SCC, Lung, Cancer

Introduction

With over 160,000 deaths annually, lung cancer is the leading cause of cancer-related deaths in the USA [1]. This is largely due to a lack of sensitive and specific diagnostic methods, as more than 60 % of patients remain undiagnosed until the disease has

Mohamed Hassanein and Matthew R. Hight contributed equally to this work.

Electronic supplementary material The online version of this article (doi:10.1007/s11307-015-0862-4) contains supplementary material, which is available to authorized users.

Correspondence to: H. Manning; *e-mail:* henry.c.manning@vanderbilt.edu

progressed to an advanced or metastatic stage [2]. To date, 2-deoxy-2-[18F]fluoro-D-glucose ([18F]FDG) positron emission tomography (PET) remains the only molecular imaging approach clinically approved for the detection and diagnosis of lung cancer. While [18F]FDG PET has proven sensitive towards the detection of glucose-avid tumors, its specificity is limited in the context of lung cancer due to an inability to distinguish cancerous lesions from inflammatory and benign nodules [3]. Alternatively, PET imaging diagnostics that measure the amino acid dependency of lung cancer cells have been reported, such as the use of radiolabeled tyrosine derivatives to access system *L* activity [4], and show promise as alternatives to [18F]FDG PET. However, the transport and metabolism of other amino acid fuel sources that may be crucial for cancer growth and development, such as glutamine, remain largely unexplored as imaging targets in lung cancer.

Emerging evidence suggests that glutamine metabolism plays a crucial role in cancer cell growth and is regulated by oncogenic signaling pathways [5–7]. In lung cancer, pharmacological inhibition of glutamine uptake has been shown to suppress cell growth *in vitro* and induce regression of primary and metastatic tumors *in vivo* [8–10]. Related to this, our group has previously identified alanine-serine-cysteine transporter 2 (ASCT2), a sodium-dependent neutral amino acid transporter of glutamine that is encoded by the gene *SLC1A5*, to both be expressed in a majority of lung cancers and found ASCT2 to be the primary transporter of glutamine in cell lines of human non-small cell lung cancer (NSCLC) [11]. Furthermore, pharmacological inhibition of ACT2 was found to attenuate both cell growth and the mTOR signaling pathway. From more recent studies, expression of ASCT2 was also linked to poor survival rate in lung cancer cells [12].

Given these findings, we hypothesized that a quantitative PET measure of ASCT2 expression and glutamine metabolism could have potential as a precision imaging diagnostics of lung cancer. In these studies, we evaluated a previously described fluorine-18 radiolabeled analogue of glutamine, (2*S*,4*R*)-4-[18F]fluoroglutamine [13], henceforth referred to as 4-[18F]fluoro-Gln, as a quantitative measure of ASCT2 expression in human cell line xenografts of varying transporter levels and a genetically engineered epidermal growth factor receptor (EGFR)-mutant mouse model of lung cancer. Comparisons were also made to the current clinical standard, [18F]FDG PET.

Materials and Methods

Small Animal Models

All studies involving small animals were conducted in accordance with both federal and institutional guidelines. Human xenograft small animal models were developed through subcutaneous injection of H520 lung squamous cell carcinoma (SCC) cells (2×10^6), COLO-205 colorectal cancer (CRC) cells (1×10^7), or HCT-116 CRC cells (1×10^7) into the right flank of 6- to 8-week-old athymic nude mice (6904F, Harlan). Palpable tumors were observed within 90 days for H520 tumors or 3 to 4 weeks for COLO-205 and HCT-116 tumors following inoculation and selected for PET imaging upon tumors reaching a minimum size of 100 mm^3, as was determined using caliper measurements of sagittal tumor sections.

The generation of $Egfr^{L858R}$ and $Egfr^{L858R+T790M}$ NSCLC mice, male and female, was performed as described previously [14]. Briefly, expression of tetracycline-regulated oncogenes in lung epithelia was induced in bitransgenic mice through feeding of doxycycline-impregnated chow (625 ppm; Harlan-Teklad) after genotype confirmation via tail biopsies. Mice began developing tumors within 6 weeks as was apparent by the appearance of ruff hair coat, rapid shallow breathing, and weight loss. Tumor burden was confirmed using anatomical magnetic resonance imaging at 8 weeks.

Radiochemistry, PET Imaging, and Analysis

[18F]FDG was obtained from a commercial vendor. 4-[18F]fluoro-Gln was produced using a methodology analogous to those previously reported [13, 15]. Imaging acquisition and processing were performed analogously to our previously reported methods [16]. Further details on these methods are provided in the supporting information (SI).

Immunoblotting and Immunohistochemistry

Detailed immunoblotting and immunohistochemistry (IHC) methods can be found in the SI.

Statistical Analysis

The mean radiotracer concentration within each ROI between 40 and 60 min post radiotracer administration were used for statistical analysis. Statistical significance of tumor-to-muscle comparisons in xenograft tumor models was evaluated using a paired, two-tailed *t* test. Similarly, tumor-to-lung, tumor-to-heart, and lung-to-heart comparisons in $Egfr^{L858R+T790M}$ transgenic mice were compared using an unpaired, two-tailed *t* test. Differences were assessed within the GraphPad Prism software (v.6.01) package and considered statistically significant if p values were less than 0.05.

Results

4-[18F]Fluoro-Gln in Xenograft Tumor-Bearing Mice

To explore the potential of PET imaging to non-invasively evaluate ASCT2 expression in tumors, we evaluated 4-[18F]fluoro-Gln accumulation in three distinct cell line xenograft tumors of varying ASCT2 expressions: H520 (SCC, $n=4$), COLO-205 (CRC, $n=9$), and HCT-116 (CRC, $n=5$). Following administration, 4-[18F]fluoro-Gln exhibited preferential accumulation in sites of tumor growth, relative to muscle, for all xenograft models (Fig. 1a). Mean tracer uptake, as determined by injected dose per cc (%ID/cc), was

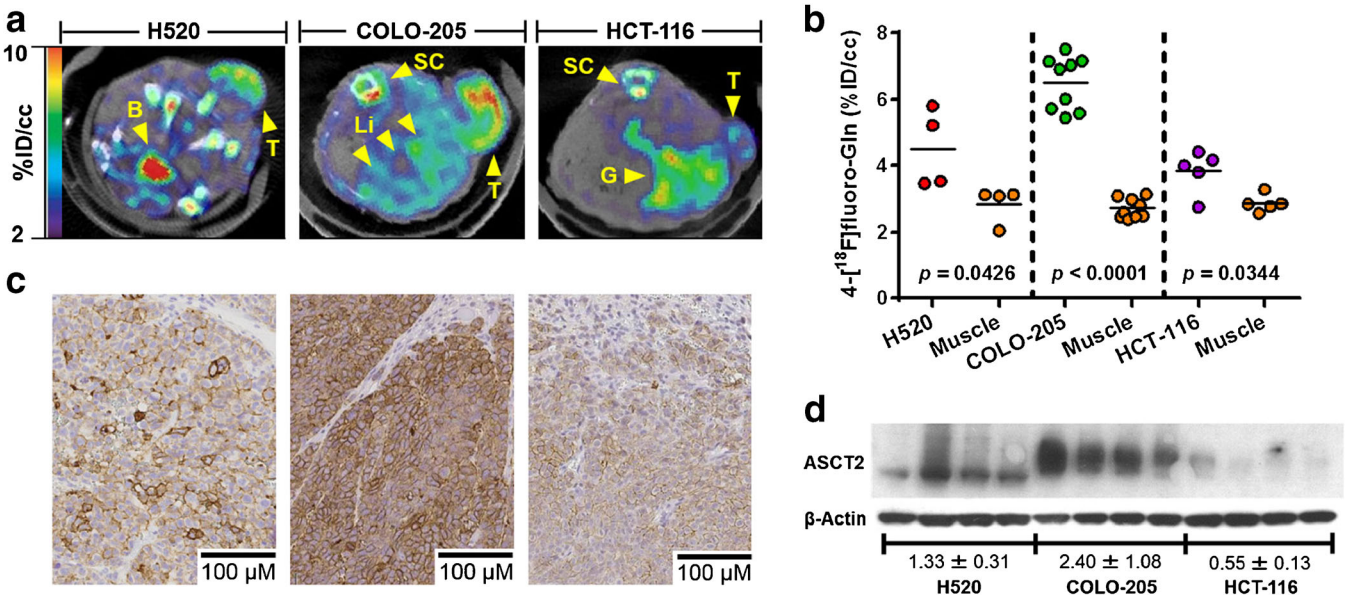

Fig. 1 4-[18F]Fluoro-Gln screening in lung and colon xenograft tumors. **a** Representative 4-[18F]fluoro-Gln transverse PET images, summed from the last 20 min of the 60-min scan, and co-registered CT images of athymic nude mice bearing H520, COLO-205, and HCT-116 xenograft tumors. *Yellow arrows* denote the location of the xenograft tumor (*T*), bladder (*B*), spinal column (*SC*), liver (*Li*), and gut (*G*). **b** Individual tracer accumulation for tumor and matched muscle in tumor-bearing mice demonstrated significant uptake in all tumor models (>3.5 %ID/cc). Representative high-power white-light images (20×) of ASCT2 immunohistochemical staining in resected tumor tissue as well as immunoblotting evaluation in tumor lysate, **c** and **d** respectively, revealed ASCT2 expression levels which trended with observations gained from 4-[18F]fluoro-Gln PET. Semi-quantitative densitometric measurements of ASCT2 band intensity, normalized to corresponding B-actin bands, were performed using the public domain image processing software ImageJ and shown as the mean relative intensity with standard deviation (*n*=4).

found to be statistically different, using a paired Student's *t* test, between tumor and muscle tissues for H520 (4.51±1.18 %ID/cc, p=0.0426), COLO-205 (6.51±0.80 %ID/cc, p<0.0001), and HCT-116 (3.83±0.64 %ID/cc, p=0.0344) (Fig. 1b). Histological evaluation of the ASCT2 expression in harvested xenograft tumors illustrated detectable transporter expression, compared to surrounding stroma, which varied in intensity among the three tumor models (Fig. 1c). Notably, overall 4-[18F]fluoro-Gln uptake in xenograft tumor tissue agreed with relative ASCT2 expression levels by both histology and immunoblotting analysis (Fig. 1d). By comparison, [18F]FDG accumulation did not exceed background muscle accumulation in H520 lung cancer xenografts (3.30±0.14 %ID/cc, p=0.8099) (Fig. 2), and as expected, [18F]FDG did not agree with relative ASCT2 expression. In both CRC xenograft tumor models, [18F]FDG tumor uptake was comparable or greater than 4-[18F]fluoro-Gln (4.72±0.86 %ID/cc, p<0.0001 for COLO-205 and 5.23±0.68 %ID/cc, p<0.0001 for HCT-116).

ASCT2 Expression in EGFR-Mutant Tissues and Cells

Building upon the cell line xenograft studies and serving as a bridge to preclinical imaging studies in genetically engineered mouse models of lung cancer, ASCT2 expression was explored in epidermal growth factor receptor (EGFR)-mutant human lung cancers. IHC analysis was performed in tumor and matched normal tissue samples obtained from four Vanderbilt patients confirmed to exhibit the EGFR mutation. ASCT2 was found to be significantly elevated in areas of cancer growth, compared to the normal lungs, with predominantly membranous distribution (Fig. 3a).

To further evaluate ASCT2 expression in human lung cancer harboring the EGFR mutation, we evaluated its expression in parental and erlotinib-resistant EGFR-mutant

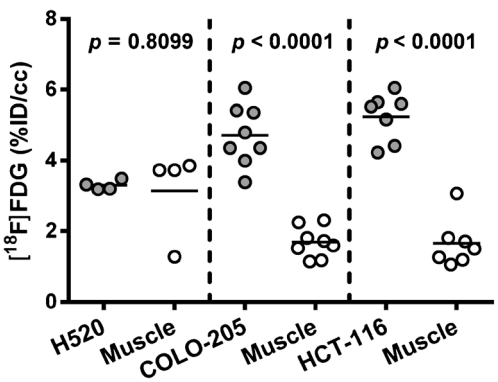

Fig. 2 [18F]FDG screening in lung and colon xenograft tumors. Individual tracer accumulation for tumor and matched muscle in tumor-bearing mice demonstrated significant uptake in both CRC tumor models (>4.5 %ID/cc) but not for lung H520 tumors, in which tracer accumulation was comparable to background.

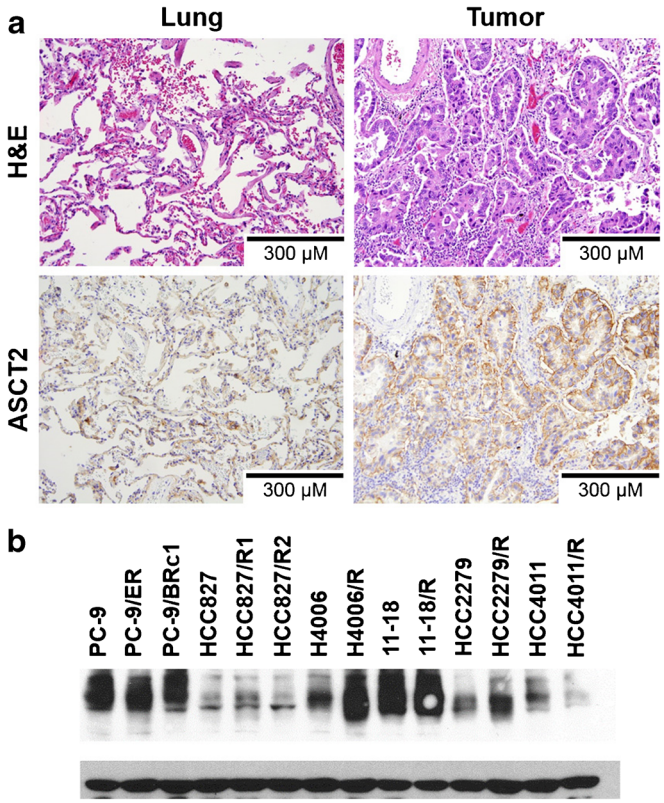

Fig. 3 ASCT2 is overexpressed in human NSCLC. **a** Representative high-power white-light images (20×) of the hematoxylin and eosin (H&E)- and ASCT2-stained normal lung and *EGFR*$^{L858R+T790M}$ human lung tumor tissues. ASCT2 staining revealed elevated levels of transporter expression in sites of NSCLC growth. **b** Immunoblotting of ASCT2 expression in human NSCLC cell lines harboring the *EGFR*$^{L858R+T790M}$ mutation.

NSCLC cell lines derived previously using well-established, *in vivo* dose-escalation protocols [17, 18]. Immunoblotting evaluation revealed ASCT2 to be overexpressed in EGFR-mutant cell lines (PC9, H4006, H2279) compared to immortalized human bronchial epithelial cells (HBE) (Fig. 3b). Collectively, these results suggest that ASCT2 is differentially expressed in EGFR-mutant NSCLC tissues and cell lines. As such, these findings provided the rationale for investigating 4-[^{18}F]fluoro-Gln PET in the *Egfr*$^{L858R+T790M}$ transgenic mouse model as a new, potentially translational molecular imaging strategy in NSCLC.

4-[^{18}F]Fluoro-Gln in Egfr$^{L858R+T790M}$ Lung Tumors

The ability of 4-[^{18}F]fluoro-Gln to image tumors arising spontaneously in the lung was evaluated in genetically engineered *Egfr*$^{L858R+T790M}$ mice (n=4) [14], which mimic NSCLC, along with wild-type control littermates (n=4). Upon administration, 4-[^{18}F]fluoro-Gln exhibited preferential accumulation in lung tumors (8.64±0.88 %ID/cc) (Fig. 4a). Importantly, 4-[^{18}F]fluoro-Gln exhibited modest accumulation in the normal lung (3.05±1.13 %ID/cc) and cardiac (4.32±1.01 %ID/cc) tissue in wild-type mice relative to *Egfr*$^{L858R+T790M}$ tumors (p=0.0002 and p=0.0007, respectively) (Fig. 4b). Mean 4-[^{18}F]fluoro-Gln time activity curves (TACs) for all mice (n≥4) revealed rapid tracer delivery in the tumor, normal lung, and heart with each tissue exhibiting a unique clearance profile (Fig. 4c). Based on %ID/cc, a tumor-to-lung ratio of 3:1 was achieved by conclusion of the 60-min scan. Dissimilar from the uptake trends observed in H520 SCC xenografts, [^{18}F]FDG accumulated preferentially in *Egfr*$^{L858R+T790M}$ tumors (17.50±3.19 %ID/cc, n=5) in a manner similar to 4-[^{18}F]fluoro-Gln (Fig. 4a). However, in contrast to 4-[^{18}F]fluoro-Gln, [^{18}F]FDG showed strong accumulation in cardiac tissue (8.40±3.90 %ID/cc) compared to the normal lung (2.46±0.32 %ID/cc, p=0.0229) (Fig. 4b). Mean [^{18}F]FDG TACs of all mice imaged (n≥4) illustrated rapid and increasing tracer delivery in tumor and lung tissues with minimal clearance from tumor tissue, as opposed to the lungs which exhibited a steady clearance profile (Fig. 4c). In this model, [^{18}F]FDG showed a higher tumor-to-lung ratio (7:1), compared to 4-[^{18}F]fluoro-Gln, by the conclusion of the 60-min scan. Histological evaluation revealed ASCT2 to be expressed in cancerous tissue regions (Fig. 4d).

Discussion

In these studies, we sought to evaluate 4-[^{18}F]fluoro-Gln, a previously reported fluorine-18 radiolabeled analogue of

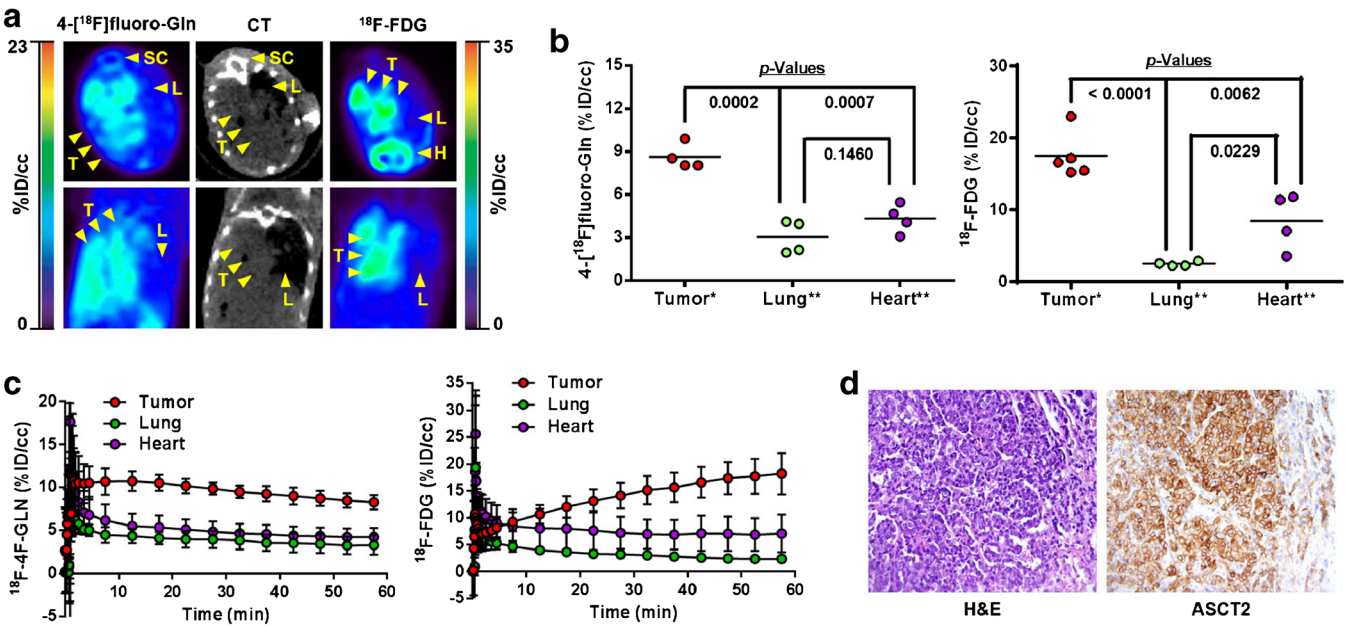

Fig. 4 4-[18F]Fluoro-Gln PET agreed with ASCT2 expression in $Egfr^{L858R+T790M}$-driven lung tumors. **a** Representative 4-[18F]fluoro-Gln and [18F]FDG transverse (*top*) and coronal (*bottom*) PET images, summed from the last 20 min of the 60-min scan, and matching CT in a transgenic mouse bearing $Egfr^{L858R+T790M}$ lung tumors. *Yellow arrows* and *text* denote the location of the tumor (*T*), normal lung (*L*), spinal column (*SC*), and heart (*H*). Individual tracer accumulation and TACs for the tumor and normal lung in transgenic mice, **b** and **c** respectively, demonstrated considerable uptake of each tracer compared to the normal lung; "*" represents genetically engineered mice and "**" represents wild-type mice. **d** Representative high-power white-light images (20×) of the H&E- and ASCT2-stained normal lung and tumor tissues resected from $Egfr^{L858R+T790M}$ mice revealed expression of ASCT2 which agreed with 4-[18F]fluoro-Gln PET.

glutamine [13], as a quantitative measure of ASCT2 expression in small animal models of lung cancer. Initially, 4-[18F]fluoro-Gln accumulation was screened using preclinical PET of human cell line xenograft mouse models of cancer, each of which possessed different levels of transporter expression. Comparatively, all three xenograft models exhibited elevated tracer accumulation, compared to muscle, and agreed with ASCT2 histological and immunoblotting evaluations. From these studies, the CRC cell line COLO-205 displayed the highest degree of tracer accumulation in tumor tissue, followed by the lung cancer cell line H520 and the CRC cell line HCT-116. Trends in 4-[18F]fluoro-Gln accumulation agreed with the relative levels of ASCT2 expression that were observed in excised tumor tissue by immunoblotting and IHC. Interestingly, tumor accumulation trends for [18F]FDG differed from those observed for 4-[18F]fluoro-Gln in that accumulation in lung cancer H520 tumors was not discernable from background.

To explore glutamine PET in a more clinically relevant setting, 4-[18F]fluoro-Gln was explored as a measure of ASCT2 expression in a genetically engineered mouse model that recapitulates many features of human EGFR-mutant lung cancer. 4-[18F]Fluoro-Gln was observed to accumulate at higher rates in sites of NSCLC tumor growth, compared to both the normal lung and cardiac tissue, but exhibited modest tumor tissue wash-out over the course of a 60-min uptake period. Interestingly, heart-to-lung contrast for [18F]FDG was high, as opposed to 4-[18F]fluoro-Gln, and suggests that 4-[18F]fluoro-Gln PET of lung tissue would not suffer from cardiac tissue signal spillover.

While these studies provide an initial evaluation of 4-[18F]fluoro-Gln PET imaging as a means to assess ASCT2 expression in lung cancer, the potential of this diagnostic approach to serve as an alternative to [18F]FDG PET requires further exploration. Future studies should compare 4-[18F]fluoro-Gln and [18F]FDG PET in a setting that more rigorously evaluates these tracers for specificity to cancerous lesions over inflammatory and/or benign lung nodules of similar size. It is well-established that [18F]FDG PET lacks the specificity needed to diagnose lung cancer in the setting of indeterminate pulmonary nodules due to accumulation in inflammatory lesions [19]. A potential limitation of 4-[18F]fluoro-Gln is its lack of ASCT2 selectivity. Glutamine accumulation in cells is accomplished through an evolutionarily redundant repertoire of transporters, and 4-[18F]fluoro-Gln can be internalized by the glutamine transporters beyond ASCT2 [13]. Furthermore, in a recent report, SiRNA knockdown of the transporter only resulted in reduction of 4-[18F]fluoro-Gln uptake by only 50 % [20]. Given this, another approach could explore tracers that exhibit greater ASCT2 selectivity, although these classes of probes are still in their infancy [21]. An additional reported drawback of 4-[18F]fluoro-Gln includes tracer metabolism leading to defluorination and bone accumulation [22], although we did not observe sufficient levels of defluorination in this study to hinder lung cancer imaging.

Conclusions

In preclinical studies, 4-[^{18}F]fluoro-Gln PET was found to reflect ASCT2 expression in lung and CRC human xenograft tumors, thus revealing it as a potential precision imaging diagnostics of lung cancer. Further studies should evaluate its performance in additional models of lung disease, including benign and inflammatory lung nodules.

Acknowledgments. This work was supported by the Lung Cancer Research Foundation (LCRF), Vanderbilt Center for Molecular Probes (VCMP), NIH (ICMIC P50-CA128323, 2RO1CA102353, U01CA152662, P50-CA090949, P50-CA128323, P30-DK058404), and Kleberg Foundation.

Conflict of Interest. The authors declare that they have no conflict of interest.

References

1. Edwards BK, Noone AM, Mariotto AB et al (2014) Annual Report to the Nation on the status of cancer, 1975-2010, featuring prevalence of comorbidity and impact on survival among persons with lung, colorectal, breast, or prostate cancer. Cancer 120:1290–1314
2. Parkin DM, Bray F, Ferlay J, Pisani P (2005) Global cancer statistics, 2002. CA Cancer J Clin 55:74–108
3. Deppen S, Putnam JB Jr, Andrade G et al (2011) Accuracy of FDG-PET to diagnose lung cancer in a region of endemic granulomatous disease. Ann Thorac Surg 92:428–432, **discussion 433**
4. Burger IA, Zitzmann-Kolbe S, Pruim J et al (2014) First clinical results of (D)-18F-Fluoromethyltyrosine (BAY 86-9596) PET/CT in patients with non-small cell lung cancer and head and neck squamous cell carcinoma. J Nucl Med 55:1778–1785
5. Liu W, Le A, Hancock C et al (2012) Reprogramming of proline and glutamine metabolism contributes to the proliferative and metabolic responses regulated by oncogenic transcription factor c-MYC. Proc Natl Acad Sci U S A 109:8983–8988
6. Gaglio D, Metallo CM, Gameiro PA et al (2011) Oncogenic K-Ras decouples glucose and glutamine metabolism to support cancer cell growth. Mol Syst Biol 7:523
7. Wang JB, Erickson JW, Fuji R et al (2010) Targeting mitochondrial glutaminase activity inhibits oncogenic transformation. Cancer Cell 18:207–219
8. Brower M, Carney DN, Oie HK, Gazdar AF, Minna JD (1986) Growth of cell lines and clinical specimens of human non-small cell lung cancer in a serum-free defined medium. Cancer Res 46:798–806
9. Drogat B, Bouchecareilh M, North S et al (2007) Acute L-glutamine deprivation compromises VEGF-a upregulation in A549/8 human carcinoma cells. J Cell Physiol 212:463–472
10. Shelton LM, Huysentruyt LC, Seyfried TN (2010) Glutamine targeting inhibits systemic metastasis in the VM-M3 murine tumor model. Int J Cancer 127:2478–2485
11. Hassanein M, Hoeksema MD, Shiota M et al (2013) SLC1A5 mediates glutamine transport required for lung cancer cell growth and survival. Clin Cancer Res 19:560–570
12. Hassanein M, Qian J, Hoeksema MD, et al (2015) Targeting SLC1A5-mediated glutamine dependence in non-small cell lung cancer. Int J Cancer. doi:10.1002/ijc.29535
13. Qu W, Zha Z, Ploessl K et al (2011) Synthesis of optically pure 4-fluoro-glutamines as potential metabolic imaging agents for tumors. J Am Chem Soc 133:1122–1133
14. Regales L, Balak MN, Gong Y et al (2007) Development of new mouse lung tumor models expressing EGFR T790M mutants associated with clinical resistance to kinase inhibitors. PLoS One 2, e810
15. Qu W, Oya S, Lieberman BP et al (2012) Preparation and characterization of L-[5-11C]-glutamine for metabolic imaging of tumors. J Nucl Med 53:98–105
16. Hight MR, Cheung YY, Nickels ML et al (2014) A peptide-based positron emission tomography probe for in vivo detection of caspase activity in apoptotic cells. Clin Cancer Res 20:2126–2135
17. Chmielecki J, Foo J, Oxnard GR et al (2011) Optimization of dosing for EGFR-mutant non-small cell lung cancer with evolutionary cancer modeling. Sci Transl Med 3:90ra59
18. Ohashi K, Maruvka YE, Michor F, Pao W (2013) Epidermal growth factor receptor tyrosine kinase inhibitor-resistant disease. J Clin Oncol 31:1070–1080
19. Deppen SA, Blume JD, Kensinger CD et al (2014) Accuracy of FDG-PET to diagnose lung cancer in areas with infectious lung disease: a meta-analysis. JAMA 312:1227–1236
20. Venneti S, Dunphy MP, Zhang H et al (2015) Glutamine-based PET imaging facilitates enhanced metabolic evaluation of gliomas in vivo. Sci Transl Med 7:274ra217
21. Schulte ML, Dawson ES, Saleh SA, Cuthbertson ML, Manning HC (2015) 2-Substituted Nγ-glutamylanilides as novel probes of ASCT2 with improved potency. Bioorg Med Chem Lett 25:113–116
22. Wu Z, Zha Z, Li G, et al (2014) [(18)F](2S,4S)-4-(3-Fluoropropyl)glutamine as a tumor imaging agent. Mol Pharm 11(11):3852–3866